Substitution Reactions of $(C_5Ph_5)Cr(CO)_3$: Structural, Electrochemical, and Spectroscopic Characterization of $(C_5Ph_5)Cr(CO)_2L$ (L = PMe_3, PMe_2Ph, $P(OMe)_3$)

D. John Hammack,[1a] Mills M. Dillard,[1a] Michael P. Castellani,*[,1a] Arnold L. Rheingold,*[,1b] Anne L. Rieger,[1c] and Philip H. Rieger*[,1c]

Departments of Chemistry, Marshall University, Huntington, West Virginia 25755, University of Delaware, Newark, Delaware 19716, and Brown University, Providence, Rhode Island 02912

Received May 20, 1996[⊗]

The radical complex $(C_5Ph_5)Cr(CO)_3$ reacts with small, neutral, monodentate Lewis bases (PMe_3, PMe_2Ph, $P(OMe)_3$) in THF at −78 °C (PMe_2Ph reacts at ambient temperature) to yield the monomeric substitution products $(C_5Ph_5)Cr(CO)_2L\cdot THF$ as thermally stable solids. Electrochemical and spectroscopic data are provided. An X-ray crystal structure of the hemisolvate $(C_5Ph_5)Cr(CO)_2PMe_3\cdot 0.5THF$ was obtained. Frozen-solution ESR spectra of $(C_5Ph_5)Cr(CO)_2L$ in toluene are comparable to those of other low-spin d^5 "piano-stool" complexes. Rotation of the $Cr(CO)_2L$ moiety relative to the C_5Ph_5 ring is rapid on the ESR time scale in low-temperature liquid solutions and leads to axial powderlike spectra. Analysis of this effect leads to significant insights into the electronic structure.

Introduction

Over the past two decades, the study of paramagnetic organometallic complexes has greatly expanded.[2] These complexes are generally highly reactive, and many have been postulated as reaction intermediates. In particular, the $(C_5R_5)Cr(CO)_3$ (R = H, Me, Ph) family of complexes recently has received much attention. The R = H and Me complexes both exist in equilibria between 17e monomers and 18e dimers in solution and as dimers in the solid state,[3] while for R = Ph the complex exists solely as a 17e monomer both in solution and the solid state.[4]

Seventeen electron complexes containing CO ligands frequently undergo substitution reactions under mild conditions.[5,6] The reactions tend to proceed via associative mechanisms[7] because of incompletely filled sets of bonding molecular orbitals.[8] Baird and co-workers have studied extensively the substitution reactions of $(C_5R_5)Cr(CO)_3$ (R = H,[9] Me[9e,10]) with phosphines. Where R = H (Cp) isolation of a product complex requires larger phosphines, while for R = Me (Cp*) only smaller phosphines replace CO in the starting complex.

The very large size of the C_5Ph_5 ligand should significantly restrict the size of substituents that can substitute CO in $(C_5Ph_5)Cr(CO)_3$, **1**. Three small, monodentate Lewis bases, PMe_3, PMe_2Ph, and $P(OMe)_3$, react with **1** to yield isolable products, $(C_5Ph_5)Cr(CO)_2L$. These compounds have been spectroscopically and electrochemically characterized.

There have been many ESR studies of low-spin d^5 "piano-stool" complexes such as $(C_5R_5)Cr(CO)_{3-x}L_x$ (R = H, Me), $[(arene)Cr(CO)_{3-x}L_x]^+$, and Mn(II) analogs.[11] As we will show, the ESR spectra of $(C_5Ph_5)Cr(CO)_2L$ fit comfortably into the general scheme for these complexes and are thus rather unremarkable. However, the unique steric bulk of the C_5Ph_5 ligand leads to selective averaging of anisotropies in the ESR spectra of low-temperature liquid solutions, and parameters obtained from such spectra provide insights into the electronic structure which were unavailable in previous studies.

⊗ Abstract published in *Advance ACS Abstracts,* September 15, 1996.

(1) (a) Marshall University. (b) University of Delaware. (c) Brown University.

(2) (a) Connelly, N. G.; Geiger, W. C. *Adv. Organomet. Chem.* **1984**, *23*, 1. (b) Baird, M. C. *Chem. Rev.* **1988**, *88*, 1217. (c) Astruc, D. *Chem. Rev.* **1988**, *88*, ll89. (d) *Organometallic Radical Processes*; Trogler, W. C., Ed.; Elsevier: Amsterdam, 1990.

(3) (a) Adams, R. D.; Collins, D. E.; Cotton, F. A. *J. Am. Chem. Soc.* **1974**, *96*, 749. (b) McLain, S. J. *J. Am. Chem. Soc.* **1988**, *110*, 643. (c) Goh, L. Y.; Khoo, S. K.; Lim, Y. Y. *J. Organomet. Chem.* **1990**, *399*, 115. (d) Goh, L. Y.; Hambley, T. W.; Darensbourg, D. J.; Reibenspies, J. *J. Organomet. Chem.* **1990**, *381*, 349. (e) Watkins, W. C.; Jaeger, T.; Kidd, C. E.; Fortier, S.; Baird, M. C.; Kiss, G.; Roper, G. C.; Hoff, C. D. *J. Am. Chem. Soc.* **1992**, *114*, 907. (f) The fluorenyl complex $(C_{13}H_9)Cr(CO)_3$ has also been prepared. It is also unstable and undergoes a $Cr(CO)_3$ shift from the C_5 ring to a C_6 ring, followed by a dimerization through the methine C_5 carbon. Novikova, L. N.; Ustynyuk, N. A.; Tumanskii, B. L.; Petrovskii, P. V.; Borisenko, A. A.; Kukharenko, S. V.; Strelets, V. V. *Isv. Akad. Nauk, Ser. Khim.* **1995**, 1354 (*Russ. Chem. Bull., Engl. Transl.* **1995**, *44*, 1306).

(4) Hoobler, R. J.; Hutton, M. A.; Dillard, M. M.; Castellani, M. P.; Rheingold, A. L.; Rieger, A. L.; Rieger, P. H.; Richards, T. C.; Geiger, W. E. *Organometallics* **1993**, *12*, 116.

(5) (a) Kochi, J. K. *Organometallic Mechanisms and Catalysis*; Academic: New York, 1978; Chapter 8. (b) Reference 2d, Chapters 4 and 9.

(6) Huang, Y.; Carpenter, G. B.; Sweigart, D. A.; Chung, Y. K.; Lee, B. Y. *Organometallics* **1995**, *14*, 1423.

(7) (a) Atwood, J. D. *Inorganic and Organometallic Reaction Mechanisms*; Brooks/Cole: Monterey, CA, 1985; p 123. (b) Crabtree, R. H. *The Organometallic Chemistry of the Transition Metals*; John Wiley and Sons: New York, 1988; pp 80−81.

(8) (a) Therien, M. J.; Trogler, W. C. *J. Am. Chem. Soc.* **1988**, *110*, 4942. (b) Lin, Z.; Hall, M. B. *Inorg. Chem.* **1992**, *31*, 2791.

(9) (a) Cooley, N. A.; Watson, K. A.; Fortier, S.; Baird, M. C. *Organometallics* **1988**, *7*, 2563. (b) Cooley, N. A.; MacConnachie, P. T. F.; Baird, M. C. *Polyhedron* **1988**, *7*, 1965. (c) Cooley, N. A.; Baird, M. C.; Morton, J. R.; Preston, K. F.; Le Page, Y. *J. Magn. Reson.* **1988**, *76*, 325. (d) Watkins, W. C.; Macartney, D. H.; Baird, M. C. *J. Organomet. Chem.* **1989**, *377*, C52. (e) Fortier, S.; Baird, M. C.; Preston, K. F.; Morton, J. R.; Ziegler, T.; Jaeger, T. J.; Watkins, W. C.; MacNeil, J. H.; Watson, K. A.; Hensel, K.; Le Page, Y.; Charland, J.-P.; Williams, A. J. *J. Am. Chem. Soc.* **1991**, *113*, 542. (f) O'Callaghan, K. A. E.; Brown, S. J.; Page, J. A.; Baird, M. C.; Richards, T. C.; Geiger, W. E. *Organometallics* **1991**, *10*, 3119. (g) Watkins, W. C.; Hensel, K.; Fortier, S.; Macartney, D. H.; Baird, M. C.; McLain, S. J. *Organometallics* **1992**, *11*, 2418.

(10) Jaeger, T. J.; Baird, M. C. *Organometallics* **1988**, *7*, 2074.

(11) Rieger, P. H. *Coord. Chem. Rev.* **1994**, *135*, 203.

S0276-7333(96)00374-3 CCC: $12.00

Experimental Section

General Data. All reactions of air- and moisture-sensitive materials were performed under a nitrogen atmosphere employing standard Schlenk techniques unless otherwise stated. Solids were manipulated under nitrogen or argon in a Vacuum Atmospheres glovebox equipped with a HE-493 dri-train. Solvents (Fisher) were distilled from the appropriate drying agent under argon: toluene, hexane (sodium/benzophenone), benzene, tetrahydrofuran (THF) (potassium/benzophenone), and dichloromethane (CaH_2). $(C_5Ph_5)Cr(CO)_3{\cdot}C_6H_6$ was prepared according to a literature procedure.[4] NMR solvents were vacuum distilled from CaH_2 and placed under an argon atmosphere. PPh_3 (PCR) was recrystallized from 95% ethanol. PMe_3, PMe_2Ph, $P(OMe)_3$, $P(OPh)_3$ (Strem), $CDCl_3$, CD_2Cl_2 (Aldrich), 2,2′-bipyridine (Matheson), diphenylacetylene (Eastman), and all other solvents (Fisher) were used without further purification. Elemental analyses were performed by Schwartzkopf Microanalytical Laboratory, Woodside, NY, and Mickroanalytisches Labor Pascher, Remagen, Germany. ^1H (200.06 MHz) and ^{31}P (80.962 MHz) NMR spectra were obtained on a Varian XL-200 NMR spectrometer equipped with a Motorola data system upgrade.

Electrochemistry. Electrochemical data were obtained on a EG&G PAR VersaStat Model 250-1 electrochemical analysis system. The apparatus was maintained on a bench top under constant nitrogen purge. Freshly distilled CH_2Cl_2 was employed as the solvent, with a supporting electrolyte of 0.1 M $^nBu_4NPF_6$ (recrystallized from 95% ethanol). Solutions were *ca*. 3 mM in complex.[12] Decamethylferrocene was added as an internal reference. Potentials are referred to the ferrocene/ferrocenium couple. All data were obtained with a Pt disk working electrode ($r = 1.6$ mm) and either a Ag/AgCl reference electrode or a AgCl-coated Ag wire reference electrode.

ESR Spectroscopy. Electron spin resonance spectra were obtained using a Bruker ER-220D X-band spectrometer equipped with a Bruker variable-temperature accessory, a Systron-Donner microwave frequency counter, and a Bruker gaussmeter. Samples for ESR study were prepared in an argon-filled glovebox by shaking the compound with degassed toluene to obtain a saturated solution; the solution was syringed into an ESR tube which was sealed with Parafilm before removal from the glovebox. One series of spectra was obtained with 5 mg of the $P(OMe)_3$ complex in 3 mL of 1:1 1,2-$C_2H_4Cl_2$/CH_2Cl_2 (dce/dcm); the solution was prepared in a glovebox as before.

X-ray Structural Determination. Crystallographic data are summarized in Table 1. A specimen mounted on a glass fiber was found photographically to possess only triclinic symmetry. The centrosymmetric space group was initially assumed and later supported by the reasonable results of refinement. Variation in azimuthal scans were less than 10%, and corrections for absorption were ignored. The structure was solved by direct methods. The asymmetric unit is composed of two crystallographically independent but chemically very similar molecules of the Cr complex and one molecule of THF. All non-hydrogen atoms were refined with anisotropic displacement parameters. Selected bond distances and angles are collected in Tables 2 and 3, respectively. Phenyl dihedral angles are presented in Table 4. All computations used SHELXTL 4.2 programs (G. Sheldrick, Siemens XRD, Madison, WI).

Low-Temperature IR Spectroscopy. In a glovebag, a dilute solution of **1** in THF was cooled to −78 °C. Two equivalents of PMe_3 were added, and the solution was allowed to warm until the blue solution turned to a green color. The solution was recooled to −78 °C and then transferred to a precooled IR cell via a precooled syringe (both at −78 °C). The color changes observed are the same as occur in synthetic scale reactions.

$(C_5Ph_5)Cr(CO)_2PMe_3{\cdot}$THF (2). $(C_5Ph_5)Cr(CO)_3{\cdot}C_6H_6$ (0.50 g, 0.76 mmol) was dissolved in 10 mL of THF. The solution was then cooled to −78 °C, and 0.21 mL PMe_3 (2.0 mmol) was added. The solution was allowed to warm to room temperature with stirring (*ca*. 1 h). As the dark blue solution warmed, it

(12) Solutions at higher concentrations than normal were used because of the high air-sensitivity of the complexes in solution. Under the conditions employed, 0.5 mM solutions rarely maintained their integrity for more than a few minutes. Typical values of ΔE_p were in the range 150−180 mV. A 3 mM solution of $(C_5Ph_5)Cr(CO)_3$ gave the same $E°(0/1-)$ value as that reported for a much more dilute solution.[4]

Table 1. Crystal and Refinement Data for $(C_5Ph_5)Cr(CO)_2PMe_3{\cdot}0.5THF$

a. Crystal Data	
formula	$C_{40}H_{34}CrO_2P$
fw	629.6
cryst system	triclinic
space group	$P\bar{1}$
a, Å	12.834(2)
b, Å	13.271(3)
c, Å	22.536(5)
α, deg	90.96(2)
β, deg	94.29(2)
γ, deg	112.55(1)
V, Å^3	3530.6(12)
Z	4
color	dark red
cryst size, mm	0.44 × 0.58 × 0.74
D(calcd), g/cm^3	1.185
abs coeff, cm^{-1}	0.401 mm^{-1}
b. Data Collection	
diffractometer	Siemens P4
radiation	Mo Kα ($\lambda = 0.710\ 73$ Å)
temp, K	293
2*θ* scan range, deg	1.00
scan type	Wycoff
reflns collcd	14 234
obsd rflns	6465 ($F > 5.0\sigma(F)$)
c. Solution and Refinement	
solution	direct methods
refinement method	full-matrix least-squares
quantity minimized	$\sum w(F_o - F_c)^2$
weighting scheme	$w^{-1} = \sigma^2(F) + 0.0015F^2$
no. of params refined	838
final *R* indices (obsd data),%	$R = 5.62$, w$R = 6.67$
R indices (all data), %	$R = 12.75$, w$R = 8.93$
GOF	1.11
data-to-param ratio	7.7:1
largest diff peak, e Å^{-3}	0.34
largest diff hole, e Å^{-3}	−0.39

Table 2. Selected Bond Distances (Å) in $(C_5Ph_5)Cr(CO)_2PMe_3{\cdot}0.5THF$

	conformer			conformer	
	A	B		A	B
Cr−C(1)	2.254(5)	2.269(5)	Cr−P	2.383(2)	2.372(2)
Cr−C(2)	2.288(5)	2.256(4)	C(1)−C(2)	1.430(7)	1.424(7)
Cr−C(3)	2.241(6)	2.236(5)	C(2)−C(3)	1.441(8)	1.425(8)
Cr−C(4)	2.198(7)	2.212(5)	C(3)−C(4)	1.425(6)	1.430(7)
Cr−C(5)	2.218(6)	2.221(4)	C(4)−C(5)	1.429(8)	1.432(8)
Cr−CNT[a]	1.881	1.881	C(1)−C(5)	1.429(7)	1.429(8)
Cr−C(6)	1.837(6)	1.836(7)	C(6)−O(6)	1.162(7)	1.156(9)
Cr−C(7)	1.834(6)	1.812(7)	C(7)−O(7)	1.149(8)	1.158(9)

[a] CNT = centroid of the cyclopentadienyl ring.

Table 3. Bond Angles (deg) in $(C_5Ph_5)Cr(CO)_2PMe_3{\cdot}0.5THF$

	conformer			conformer	
	A	B		A	B
C(6)−Cr−C(7)	78.7(3)	78.0(4)	C(6)−Cr−CNT[a]	125.8	124.8
P−Cr−C(6)	89.4(2)	86.9(2)	C(7)−Cr−CNT	122.4	126.1
P−Cr−C(7)	89.8(2)	90.4(2)	P−Cr−CNT	134.8	133.3
OC−Cr−CO (av)	175.8(6)	176.8(7)			

[a] CNT = centroid of the cyclopentadienyl ring.

Table 4. Phenyl Ring Torsion Angles (deg) in $(C_5Ph_5)Cr(CO)_2PMe_3$·0.5THF

	conformer			conformer	
Cp carbon	A	B	Cp carbon	A	B
1	51.9	47.7	4	54.7	56.8
2	48.0	55.6	5	50.0	55.0
3	51.1	45.6			

initially turned a jade green color and then deep cherry-red. The solution was filtered via cannula and layered with 12 mL of hexane to yield **2** (0.48 g, 0.76 mmol) in 88% yield as dark red crystals: Mp 211−218 °C (dec); ^{1}H NMR (C_6D_6) δ 7.32 (m, C_5Ph_5, br) 5.76 (s, PMe_3, br); visible λ_{max} (CH_2Cl_2) 516 nm. Anal. Calcd for $C_{44}H_{42}CrO_3P$: C, 75.31; H, 6.03. Found: C, 75.69; H, 5.79.

$(C_5Ph_5)Cr(CO)_2PMe_2Ph$·THF (3). $(C_5Ph_5)Cr(CO)_3$·C_6H_6 (0.50 g, 0.76 mmol) was dissolved in 10 mL of THF, and 0.50 mL of PMe_2Ph (3.7 mmol) was added. The solution was stirred overnight. The resulting red solution was filtered via cannula and layered with 12 mL of hexane to yield **3** (0.48 g, 0.76 mmol) in 72% yield as dark red crystals: Mp 198−200 °C (dec); ^{1}H NMR (C_6D_6) δ 7.18 (m, C_5Ph_5 and $P(Me_2Ph)_3$, br), 5.49 (s, $P(Me_2Ph)_3$, br); visible λ_{max} (CH_2Cl_2) 470 nm (sh). Anal. Calcd for $C_{49}H_{44}CrO_3P$: C, 77.05; H, 5.81. Found: C, 76.54; H, 5.50.

$(C_5Ph_5)Cr(CO)_2P(OMe)_3$·THF (4). The procedure is the same as for **2** except that a magenta colored product is obtained in 90% yield: Mp 188−192 °C (dec); ^{1}H NMR (C_6D_6) δ 7.34 (m, C_5Ph_5, br), 5.32 (s, $P(OMe)_3$, br); visible λ_{max} (CH_2Cl_2) 532 nm. Anal. Calcd for $C_{44}H_{42}CrO_6P$: C, 70.49; H, 5.65. Found: C, 71.05; H, 5.06.

Results and Discussion

Syntheses. Reaction of the $(C_5Ph_5)Cr(CO)_3$ radical with a variety of neutral, monodentate Lewis bases resulted in substitution products or no reaction between the materials depending on the ligand. The small, soft ligands PMe_3 and $P(OMe)_3$ react with $(C_5Ph_5)Cr(CO)_3$ in THF solution at low temperatures to yield the substitution products, $(C_5Ph_5)Cr(CO)_2L$ (eq 1), as highly

$$(C_5Ph_5)Cr(CO)_3 + L \xrightarrow[THF]{-78\ ^\circ C} (C_5Ph_5)Cr(CO)_2L + CO \quad (1)$$

colored, crystalline materials in high yields (compounds **2** and **4**, respectively). PMe_2Ph reacts with **1** at ambient temperature to yield this product (**3**) in slighly lower yields. The former reactions proceed very rapidly at ambient temperature; however isolated yields of the products are somewhat reduced. Unlike for $CpMn(CO)_3^+$,[6,13] no evidence for disubstitution of **1** was observed. All are air-sensitive, both in solution and in the solid state. ^{1}H NMR spectra were very broad, and no resonances were observed in ^{31}P NMR spectra of these compounds.

Infrared spectral and electrochemical data for these complexes are collected in Tables 5 and 6, respectively. A cyclic voltammogram of **2** is presented in Figure 1. The CO stretching frequencies and complex reduction potentials both follow the expected trends for the ligands. In the cyclic voltammetry, the cathodic waves are assigned to a reversible, one-electron reduction, consistent with literature precedent.[9f] Two aspects of the electrochemical data are noteworthy. Replacing Cp by C_5Ph_5 in a complex usually results in potential shifts of *ca.* 0.2 V to more positive values.[4,14] In contrast, the −1/0 couples for the PMe_3 and PMe_2Ph complexes show roughly the opposite trend. Hershberger and Kochi examined a variety of $(MeCp)Mn(CO)_2L$ complexes by cyclic voltammetry and found that replacing CO by PEt_3 and $P(OMe)_3$ resulted in potential shifts of −0.70 and −0.42 V, respectively.[15] For complexes **2** and **4** the shifts are −0.85 and −0.54 V, respectively. Thus, the shifts in the reduction potentials of **2** and **4** relative to **1** are consistent with precedent. At ambient temperature, each complex also undergoes an irreversible oxidation approximately 1.3 V to more positive potential than the reversible reduction. The anodic waves equaled the cathodic waves in height within 20% in all cases and are also assigned as one-electron processes.

A low-temperature (−78 °C) infrared spectrum of the reaction mixture of **1** with excess PMe_3 shows four absorptions (Table 5). The spectrum is consistent with a compound of the formula $[(C_5Ph_5)Cr(CO)_3PMe_3][(C_5Ph_5)Cr(CO)_3]$.[16,17] It is well established that 17e complexes tend to undergo substitution reactions via associative pathways.[2d,7] Thus, a plausible reaction mechanism is shown in eqs 2 and 3. When the reaction mixture is warmed to ambient temperature, **2** is produced quantitatively (eq 4). Further studies of this and similar low-temperature reactions are underway.

$$(C_5Ph_5)Cr(CO)_3 + PMe_3 \xrightarrow{-78\ ^\circ C} (C_5Ph_5)Cr(CO)_3PMe_3 \quad (2)$$

$$(C_5Ph_5)Cr(CO)_3PMe_3 + (C_5Ph_5)Cr(CO)_3 \xrightarrow{-78\ ^\circ C} [(C_5Ph_5)Cr(CO)_3PMe_3][(C_5Ph_5)Cr(CO)_3] \quad (3)$$

$$[(C_5Ph_5)Cr(CO)_3PMe_3][(C_5Ph_5)Cr(CO)_3] \xrightarrow{PMe_3} 2(C_5Ph_5)Cr(CO)_2PMe_3 + 2CO \quad (4)$$

$PMePh_2$ reacts with **1** at ambient temperature to yield solutions which display CO absorptions in the infrared where expected but from which very little substitution product can be isolated. The following ligands do not react with **1** even at elevated temperatures (e.g. refluxing THF or benzene): PPh_3, $P(OPh)_3$, 2,2′-bipyridine, and PhC≡CPh. The data for PMe_3, PMe_2Ph, and $PMePh_2$ suggest that steric effects are probably very important in the lack of reactivity of PPh_3 and $P(OPh)_3$.

Molecular Structure of $(C_5Ph_5)Cr(CO)_2PMe_3$·0.5THF. The X-ray crystal structure of $(C_5Ph_5)Cr(CO)_2PMe_3$·0.5THF is displayed in Figure 2. Bond distances

(13) It is interesting that Baird and co-workers do not report observing evidence of disubstitution reactions occurring in isoelectronic $CpCr(CO)_3$.[6] While the large size of the C_5Ph_5 ligand probably precludes disubstitution in **1** for the ligands studied here, Baird's work suggests that a steric argument may not be necessary.

(14) (a) Broadley, K.; Lane, G. A.; Connelly, N. G.; Geiger, W. E. *J. Am. Chem. Soc.* **1983**, *105*, 2486. (b) Connelly, N. G.; Geiger, W. E.; Lane, G. A.; Raven, S. J.; Rieger, P. H. *J. Am. Chem. Soc.* **1986**, *108*, 6219. (c) Lane, G. A.; Geiger, W. E.; Connelly, N. G. *J. Am. Chem. Soc.* **1987**, *109*, 402. (d) Connelly, N. G.; Manners, I. *J. Chem. Soc., Dalton Trans.* **1989**, 283.

(15) Hershberger, J. W.; Kochi, J. K. *Polyhedron* **1983**, *2*, 929.

(16) Two absorptions, 1892 and 1791 cm^{-1}, are associated with $(C_5Ph_5)Cr(CO)_3^-$.[4] The infrared spectrum of this complex is qualitatively similar to $[(C_5Ph_5)Cr(CO)_2(depe)][(C_5Ph_5)Cr(CO)_3]$ (Jarrell, C. S.; Castellani, M. P. Unpublished results).

(17) To our knowledge no such Cr complexes are known; however, several similar Mo complexes have been isolated. The infrared spectra of the Mo complexes are very similar to those obtained for the Cr system. (a) Nolte, M. J.; Reimann, R. H. *J. Chem. Soc., Dalton Trans.* **1978**, 932. (b) Asdar, A.; Tudoret, M.-J.; Lapinte, C. *J. Organomet. Chem.* **1988**, *349*, 353.

Table 5. Infrared Spectral Data for $(C_5Ph_5)Cr(CO)_2L$ Complexes

complex	solvent	ν(C≡O),[a] cm^{-1}	ref
$(C_5Ph_5)Cr(CO)_3$	THF	2005, 1897	4
$(C_5Ph_5)Cr(CO)_2PMe_3$	THF	1911, 1797	this work
$CpCr(CO)_2PMe_3$	CH_2Cl_2	1910, 1778	9f
$(C_5Ph_5)Cr(CO)_2PMe_2Ph$	THF	1911, 1792	this work
$(C_5Ph_5)Cr(CO)_2P(OMe)_3$	THF	1923, 1816	this work
$[(C_5Ph_5)Cr(CO)_3PMe_3][(C_5Ph_5)Cr(CO)_3]$[b]	THF	2025, 1956, 1892, 1791	this work

[a] All absorptions are strong. [b] Spectrum taken at −78 °C.

Table 6. Electrochemical Data for $(C_5Ph_5)Cr(CO)_2L$ in CH_2Cl_2

complex	E_{pa}(0/1+),[a,b] V	$E°$(0/1−),[a] V	i_{pa}/i_{pc}[c]	ref
$(C_5Ph_5)Cr(CO)_3$	*ca.* 0.9[e]	−0.69	1.0	4
$(C_5H_5)Cr(CO)_2PMe_3$		−1.42		9f
$(C_5Ph_5)Cr(CO)_2PMe_3$[d]	−0.07	−1.56	0.98	this work
$(C_5H_5)Cr(CO)_2PMe_2Ph$	−0.37	−1.36		9f
$(C_5Ph_5)Cr(CO)_2PMe_2Ph$[d]	−0.06	−1.48	0.86	this work
$(C_5Ph_5)Cr(CO)_2P(OMe)_3$[d]	0.05	−1.26	0.95	this work

[a] Potential *vs* Fc. [b] Irreverisible. [c] Determined according to ref 25. [d] Scan rate 100 mV/s; 0.1 M ($^nBu_4N)PF_6$; *ca.* 3 mM complex. [e] Appears as a very broad peak. This work.

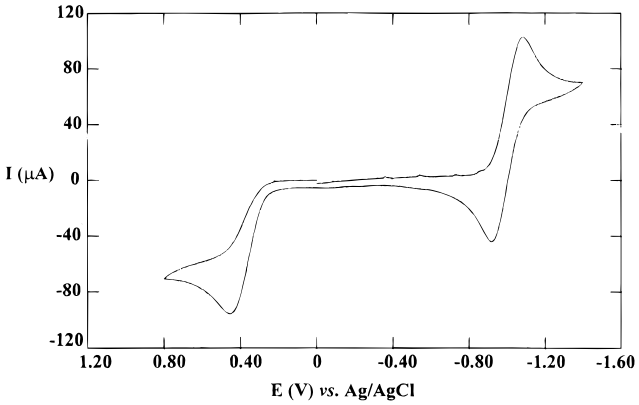

Figure 1. Cyclic voltammogram of $(C_5Ph_5)Cr(CO)_2PMe_3$ (**2**) (scan rate 100 mV/s; 0.1 M ($^nBu_4N)PF_6$; *ca.* 3 mM complex in CH_2Cl_2).

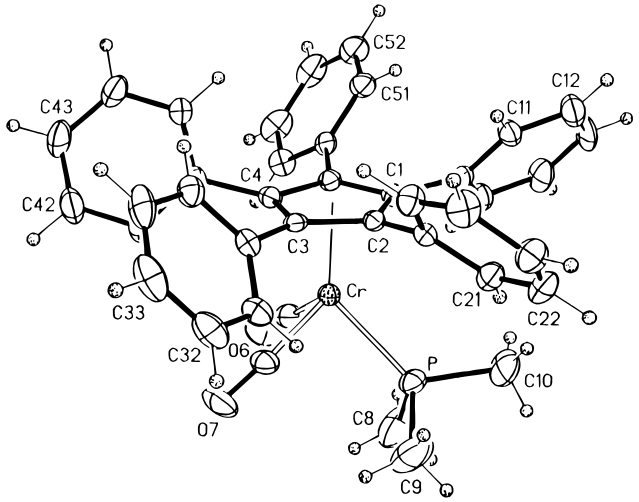

Figure 2. Molecular structure and labeling scheme for $(C_5Ph_5)Cr(CO)_2PMe_3$·0.5THF (**2**).

and angles are listed in Tables 2 and 3, respectively. Phenyl dihedral angles are given in Table 4. There are two conformers in the unit cell that do not differ in any chemically significant way. As in other, similar paramagnetic systems, the tripodal angles deviate significantly from 90°.[4,9a,e] Fortier and co-workers have reported calculations describing the origin of this effect.[9e] The P atom lies below a C−C bond of the C_5 ring (a staggered conformation). $Cp^*Cr(CO)_2PMe_3$[9e] also adopts

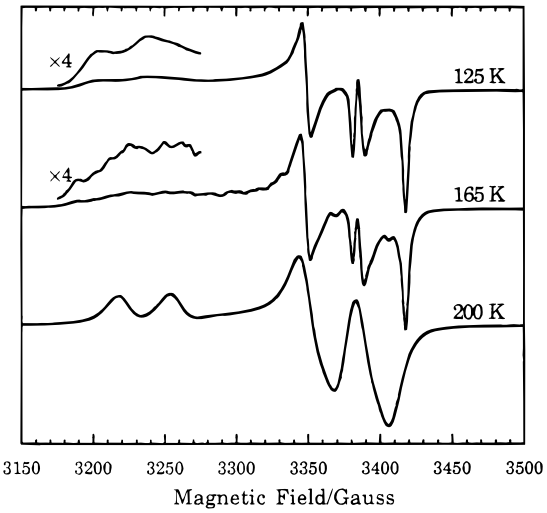

Figure 3. ESR spectra of $(C_5Ph_5)Cr(CO)_2PMe_3$ (**2**) in toluene solution at 125, 165, and 200 K. The low-field portions of the 125 and 165 K spectra are shown magnified by a factor of 4.

a staggered conformation, but for $CpCr(CO)_2PPh_3$[9a] the P atom eclipses a carbon atom of the C_5 ring. As we will show below, the conformational energy difference for **2** is small, less than or on the order of kT at 200 K (0.02 eV). One further feature of the structure warrants comment. Elemental analysis, ^1H NMR, and thermogravimetric analysis[18] all support formulation of the solid phase as a monosolvate. Since all atoms in this structure were at full occupancy, it is likely that the structure was obtained of a rare crystal of an unrepresentative solvation number.

ESR Spectra. ESR spectra of **2**−**4** in frozen toluene solution are rhombic with three distinct *g*-components. Spectra of **2** and **3** are shown in Figures 3 and 4. The spectrum of **4** is very similar to that of **2**. Interpretation of the spectra is straightforward, and the resulting parameters are given in Table 7a. In all cases, the low-field features (g_{max}) are much broader than those

(18) A TGA of this compound shows that the complex loses its THF solvate well before decomposition begins. Desolvation begins at *ca.* 150 °C and results in the crystals losing their luster with no significant decoloration occurring. Complexes **3** and **4** undergo similar visual changes for, presumably, the same reason. A copy of the TGA of **2** is provided in the Supporting Information.

Table 7. ESR Parameters for $(C_5Ph_5)Cr(CO)_2L$

(a) Frozen-Solution Spectra

L	*T*/K (solvent)	g_1	g_2	g_3	A_1[a]	A_2[a]	A_3[a]
PMe_3 (**2**)	125−160 (tol)[c]	1.9941(3)	2.0130(3)	2.104(2)	34.2(2)	35.8(4)	34(1)
PMe_2Ph (**3**)	105−120 (tol)	1.9940(2)	2.0130(2)	2.1060(2)	32.6(2)	34.8(2)	34.2(2)
$P(OMe)_3$ (**4**)	125−145 (tol)	1.9944(3)	2.0147(5)	2.130(3)	40.4(2)	45.9(2)	35(2)
$P(OMe)_3$ (**4**)	125−160 (dcm/dce)	1.9940(2)	2.0140(2)	*b*	40.2(3)	45.5(2)	*b*

(b) Liquid-Solution Spectra

L	*T*/K (solvent)	$g_\perp$	$g_\parallel$	$A_\perp$[a]	$A_\parallel$[a]
PMe_3 (**2**)	200 K (tol)	2.012(1)	2.090(1)	35(1)	35(1)
PMe_2Ph (**3**)	190 K (tol)	2.011(1)	2.091(1)	36(1)	32(2)
$P(OMe)_3$ (**4**)	180−195 K (tol)	2.006(2)	2.112(1)	46(3)	45(1)
$P(OMe)_3$ (**4**)	185 K (dcm/dce)	2.012(1)	2.095(1)	45(1)	41(1)

[a] ^{31}P hyperfine coupling in units of 10^{-4} cm^{-1}. [b] Features poorly resolved. [c] tol = toluene.

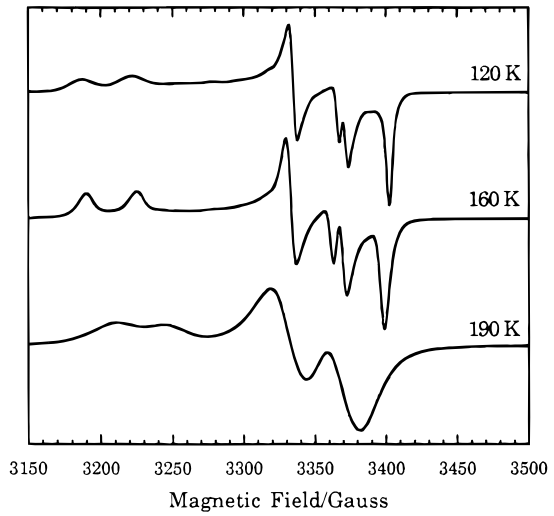

Figure 4. ESR spectra of $(C_5Ph_5)Cr(CO)_2PMe_2Ph$ (**3**) in toluene solution at 120, 160, and 190 K.

corresponding to the two smaller *g* components. For **2** and **4**, the low-field features increase in width with increasing temperature whereas, in spectra of **3**, these features are not as broad and sharpen slightly with increasing temperature. Spectra of **4** in dcm/dce were essentially identical to those in toluene except that the low-field features were broader and could not be located accurately, even at 125 K. These line width effects will be discussed elsewhere.[19]

The *g*-matrices have one component close to the free-electron *g*-value, g_e, a second component slightly larger than g_e, and a third component substantially larger than g_e. This pattern is characteristic of low-spin d^5 systems[11] and can be understood qualitatively in terms of a simple ligand-field theory model. The degeneracy of the octahedral ligand-field configuration, t_{2g}^5, is lifted in lower symmetry, but strong spin−orbit coupling of the singly-occupied orbital (SOMO) with the other two components of the t_{2g} set leads to two *g*-components greater than g_e; the third *g*-component differs from g_e through spin−orbit coupling with one of the e_g orbitals which is empty and at much higher energy. Although the spectra of $(C_5Ph_5)Cr(CO)_2L$ fit this qualitative pattern, they exhibit a temperature-dependent line width effect which requires a more detailed analysis. Furthermore, the spectra in liquid solution at low temperatures are not isotropic but resemble the frozen solution spectra, albeit with significant shifts in the positions of features.

The complexes $(C_5Ph_5)Cr(CO)_2L$ have nominal C_s symmetry so that the SOMO could belong to either the a′ or a″ representation. Previous work on related systems[9e,20,21] and extended Hückel MO calculations[9e] suggest a SOMO of a″ symmetry. Taking *xz* as the plane of symmetry, the SOMO is given by eq 5.

$$|\mathrm{SOMO}\rangle = a_1|xy\rangle + a_2|yz\rangle + \ldots \quad (5)$$

Components of the *g*-matrix are given by eqs 6,[11]

$$g_{xx} = g_e + 2[a_1^2\delta_{xz} + a_2^2(\delta_{x^2-y^2} + 3\delta_{z^2})] \quad (6a)$$

$$g_{yy} = g_e + 2(a_1^2\delta_{yz} + a_2^2\delta_{xy}) \quad (6b)$$

$$g_{zz} = g_e + 2(4a_1^2\delta_{x^2-y^2} + a_2^2\delta_{xz}) \quad (6c)$$

$$g_{xz} = -2a_1a_2(\delta_{xz} + 2\delta_{x^2-y^2}) \quad (6d)$$

where, for example, $\delta_{x^2-y^2}$ is given by eq 7, in which ζ_{Cr}

$$\delta_{x^2-y^2} = \zeta_{Cr}\sum_{k\neq 0}\frac{c_{k,x^2-y^2}^{\ 2}}{E_0 - E_k} \quad (7)$$

is the spin−orbit coupling constant for Cr, $E_0 - E_k$ is the energy of the *k*th MO relative to the energy of the SOMO, and c_{k,x^2-y^2} is the LCAO coefficient of $d_{x^2-y^2}$ in the *k*th MO. EHMO calculations[19] suggest that the two highest doubly-occupied MO's, just below the SOMO in energy (the other members of the t_{2g} set), are predominantly $d_{x^2-y^2}$ and d_{z^2} in character so that δ_{xz}, δ_{yz}, $\delta_{xy} \ll \delta_{x^2-y^2}$, δ_{z^2}. Thus g_{yy} is expected to be close to g_e, but the other components should be larger. The *g*-matrix is diagonalized by rotation about the *y*-axis by the angle β, given by eq 8, where $R = a_2/a_1$ and $Q = \delta_{z^2}/\delta_{x^2-y^2}$. The

$$\tan 2\beta = \frac{-4R}{4 - R^2(1 + 3Q)} \quad (8)$$

X and *Z* principal values of the *g*-matrix then are given by eq 9. Since, experimentally, g_X is close to g_e and g_Z

(19) Castellani, M. P.; Connelly, N. G.; Rieger, A. L.; Rieger, P. H. To be published.

(20) Morton, J. R.; Preston, K. F.; Cooley, N. A.; Baird, M. C.; Krusic, P. J.; McLain, S. J. *J. Chem. Soc., Faraday Trans. 1* **1987**, *83*, 3535.

(21) Pike, R. D.; Rieger, A. L.; Rieger, P. H. *J. Chem. Soc., Faraday Trans. 1* **1989**, *85*, 3913.

$$g_{X,Z} = g_e + {a_1}^2\delta_{x^2-y^2}[4 + R^2(1 + 3Q)] \times \left\{1 \pm \sqrt{1 - \frac{48R^2Q}{[4 + R^2(1 + 3Q)]^2}}\right\} \quad (9)$$

is much larger than g_e, the square root term of eq 9 is apparently close to 1.[22]

Spectra in liquid solution 10−20 K above the melting point of the solvent appear as approximately axial powder patterns. Spectra of **2** and **3** are shown in Figures 3 and 4; again the spectrum of **4** is qualitatively similar to that of **2**, with features significantly sharper than for **3**. In all cases, the features broaden at higher temperatures and eventually coalesce into a single broad line. Although the line narrows somewhat near room temperature, ^{31}P splitting is never resolved. Parameters for the approximately axial spectra are given in Table 7b.

The parallel features in the axial spectra are shifted upfield from the frozen-solution g_Z features, and the perpendicular features are close to the position of the g_Y features of the frozen-solution spectra. So far as we are aware, this behavior is unprecedented in organometallic ESR studies although it is similar to effects observed in liquid crystal solvents.[23] At temperatures just above the melting point, the viscosity of toluene or dce/dcm is high, and it is not surprising that molecular rotation is too slow to produce an isotropic spectrum. Apparently there is some degree of averaging, however, such that the g_X and g_Y features are merged and the g_Z features somewhat shifted. The most likely explanation of this behavior is that the $Cr(CO)_2L$ moiety is nearly freely rotating relative to the C_5Ph_5 group. In other words, the very bulky "seat" of the "piano stool" is essentially stationary on the ESR time scale while the "legs" rotate freely. The bulkier PMe_2Ph ligand would be expected to impede this averaging process, and features in the approximately axial spectra of **3** are significantly broader than those of **2** or **4**.

This behavior can be simulated using the program described by Schneider and Freed.[23] Shown in Figure 5 are computer simulations using the spin Hamiltonian parameters for **2** and a 5-G Lorentzian line width. For the simulations in Figure 5a, isotropic rotational diffusion is assumed with $D_x = D_y = D_z$ ranging from 10^7 to 5×10^8 s^{-1} whereas, in Figure 5b, rotational diffusion is anisotropic with $D_x = D_y = 10^6$ s^{-1} and D_z ranging from 10^7 to 5×10^8 s^{-1}. Although isotropic rotational diffusion can lead to an approximately axial spectrum, the parallel features are very broad and both the parallel and perpendicular features shift significantly from the frozen-solution positions. We can obtain an order-of-magnitude estimate of the isotropic rotational diffusion coefficients from eqs 10. Extrapolating literature values of the viscosity of toluene[24] to 200 K, we obtain $\eta \approx 0.43$ kg m^{-1} s^{-1}. Assuming that **2** is approximately spherical with a radius of about 7 Å, $\tau_r \approx 2 \times 10^{-7}$ s, with $D \approx 7 \times 10^5$ s^{-1}, about 2 orders of magnitude slower than required to obtain an approximately axial spectrum from isotropic motion.

$$D = 1/6\tau_r \quad (10a)$$

$$\tau_r = V_h\eta/kT \quad (10b)$$

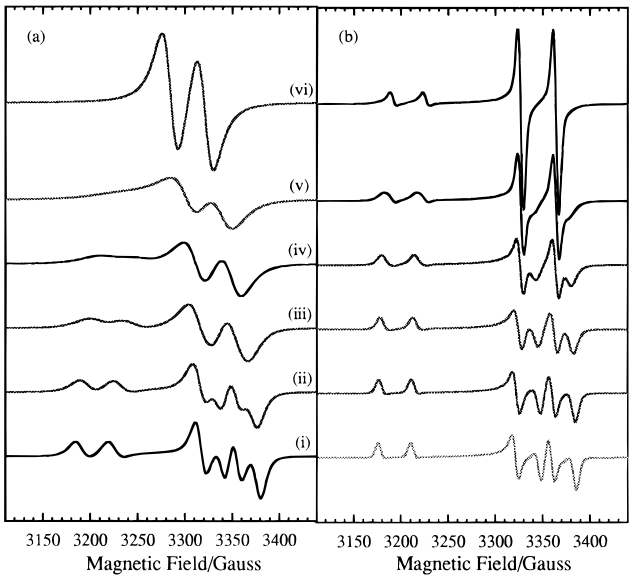

Figure 5. Simulated spectra based on the spin Hamiltonian parameters of **2**: (a) Isotropic rotational diffusion with $D_x = D_y = D_z = D$; (b) anisotropic rotational diffusion with $D_x = D_y = 10^6$ s^{-1} and $D_z = D =$ (i) 1×10^7, (ii) 2×10^7, (iii) 5×10^7, (iv) 1×10^8, (v) 2×10^8, and (vi) 5×10^8 s^{-1}.

Table 8. Values of the Angle β (deg) Computed from Axial Spectra in Toluene

	β		
L	eq 11a	eq 11b	av
PMe_3	15.3 ± 1.0	16.6 ± 1.3	15.8 ± 0.6
PMe_2Ph	15.7 ± 0.9	15.4 ± 1.4	15.6 ± 0.1
$P(OMe)_3$	15.8 ± 1.0	5.8 ± 4.8	15.4 ± 2.0

On the other hand, anisotropic rotational diffusion with $D_x = D_y \ll D_z \approx 2 \times 10^8$ s^{-1} gives a reasonable account of the experimental results. This rate is considerably faster than might have been expected for rotational diffusion of the $Cr(CO)_2PMe_3$ moiety in toluene at 200 K ($D_z \approx 3 \times 10^7$ s^{-1}, assuming a volume about $^1/_{10}$ that of the whole complex and accounting for rotation about one axis). The most likely explanation is that the "piano-stool legs" rotate in a nearly solvent-free cavity created by the C_5Ph_5 ligand.

Assuming that anisotropic rotational diffusion is fast enough to completely average g_x and g_y, that the parallel axis corresponds to the Cr−Cp vector (the *z*-axis), and that the *Z* principal axis of the *g*-matrix differs from this axis by the angle β, the parallel and perpendicular components of the averaged *g*-matrix are given by eqs 11. These equations were used to compute the values

$$2g_{\parallel}^2 = g_Z^2 + g_X^2 + (g_Z^2 - g_X^2)\cos^2 2\beta \quad (11a)$$

$$4g_{\perp}^2 = g_Z^2 + g_X^2 + 2g_Y^2 - (g_Z^2 - g_X^2)\cos^2 2\beta \quad (11b)$$

of β listed in Table 8. Except for **4**, the agreement

(22) Since EHMO calculations[19] suggest that *R* is negative and *Q* is positive, eq 9 predicts g_Z, $g_X > g_e$. The observed values of g_X, *ca.* 1.994, suggest that the δ_{xz} terms in eqs 6 are not entirely negligible.

(23) Schneider, J. H.; Freed, J. H. In *Spin Labeling: Theory and Application, Biological Magnetic Resonance, Vol. 8*; Berliner, L. J., Reuben, J., Eds.; Plenum: New York, 1989.

(24) *International Critical Tables*; Washburn, E. W., Ed.; McGraw-Hill: New York, 1926−1930; Vol. VII, p 218.

between values of β computed from $g_{\parallel}$ (eq 11a) and those computed from $g_{\perp}$ (eq 11b) is quite good, suggesting that the model is at least qualitatively correct. Extended Hückel MO calculations[19] suggest that $Q \approx 1.4$; with this value, $\beta = 16°$ and eq 8 gives $R = -0.46$, in reasonable agreement with the EHMO prediction of 0.34. The values of β listed in Table 8 also may be compared with those obtained from ESR studies of $CpCr(CO)_2PPh_3$[9c] and $(C_5Me_5)Cr(CO)_2PMe_3$[9e] diluted into single crystals of the Mn analogs. For $CpCr(CO)_2PPh_3$, four paramagnetic sites were found with slightly different principal values of the *g*-matrix and β ranging from 3 to 8°; for $(C_5Me_5)Cr(CO)_2PMe_3$, only one site was found with $\beta = 2.4°$. These angles refer to the orientation of the g_{max} principal axis relataive to the Mn−CNT axis in the host crystal and so may not be exactly equal to those relative to the Cr−CNT axis. Nonetheless, the angles are considerably smaller than those found in the present work; whether this reflects an error in our analysis or a true difference between the C_5Ph_5 ligand and the Cp and C_5Me_5 ligands is unclear.

Acknowledgment. The research at Marshall University was supported by the National Science Foundation (Grant NSF CHE-9123178) and the donors of the Petroleum Research Fund, administered by the American Chemical Society. The NSF provided funds toward the University of Delaware diffractometer. We thank Dr. R. J. Hoobler and Prof. J. W. Larson for experimental assistance, Dr. Michael Iglehart for obtaining and interpreting the TGAs, Prof. W. E. Geiger for helpful suggestions regarding both electrochemical experiments and interpretation of our results, Prof. J. H. Freed and Dr. R. Crepeau for supplying the ESR simulation program, and Prof. M. B. Zimmt for assistance in implementing the program at Brown.

Supporting Information Available: For $(C_5Ph_5)Cr(CO)_2PMe_3 \cdot 0.5THF$, listings of atomic coordinates and equivalent isotropic displacement coefficients, anisotropic displacement coefficients, and hydrogen atom coordinates (Tables 1S−3S) and a TGA diagram of **2** (12 pages). Ordering information is given on any current masthead page.

OM960374U